ECCOMAS Congress 2016
VII European Congress on Computational Methods in Applied Sciences and Engineering
M. Papadrakakis, V. Papadopoulos, G. Stefanou, V. Plevris (eds.)
Crete Island, Greece, 5–10 June 2016

A MULTI-FIDELITY ADAPTIVE SAMPLING METHOD FOR METAMODEL-BASED UNCERTAINTY QUANTIFICATION OF COMPUTER SIMULATIONS

Riccardo Pellegrini[1,2], Cecilia Leotardi[1], Umberto Iemma[2], Emilio F. Campana[1] and Matteo Diez[1]

[1]CNR-INSEAN, Natl. Research Council-Marine Technology Research Institute
Via di Vallerano 139, Rome, Italy
e-mail: c.leotardi@insean.it, {emiliofortunato.campana,matteo.diez}@cnr.it

[2] Roma Tre University, Dept. of Engineering
Via Vito Volterra 62, Rome, Italy
e-mail: {riccardo.pellegrini,umberto.iemma}@uniroma3.it

Keywords: Uncertainty Quantification, Multi-Fidelity Metamodel, Adaptive Sampling Method, Fluid-Structure Interaction.

Abstract. *A multi-fidelity global metamodel is presented for uncertainty quantification of computationally expensive simulations. The multi-fidelity approximation is built as the sum of a low-fidelity-trained metamodel and the metamodel of the difference (error) between high- and low-fidelity simulations. The metamodel is based on dynamic stochastic radial basis functions, which provide the prediction along with the associated uncertainty. New training points are added where the prediction uncertainty is largest, according to an adaptive sampling procedure. The prediction uncertainty of both the low-fidelity and the error metamodel are considered for the adaptive training of the low- and high-fidelity metamodels, respectively. The method is applied to a steady fluid-structure interaction (FSI) problem of a 3D NACA 0009 stainless steel hydrofoil. Two functions are considered simultaneously, namely lift and drag coefficients, versus angle of attack and Reynolds number. Two problems are presented: in the first problem the high-fidelity evaluations are obtained through steady FSI computer simulations, whereas in the second problem they are given by available experimental data from literature. Low-fidelity evaluations are provided in both cases by steady hydrodynamic simulations. The overall uncertainty of the multi-fidelity metamodel is used as a convergence criterion.*

1 INTRODUCTION

The simulation-based design (SBD) process of complex engineering systems (such as aerial, ground or maritime vehicles) requires computationally expensive physics-based solvers, in order to achieve accurate solutions. When dealing with real-world applications, most of the relevant inputs and outputs are affected by uncertainty, which stems from operational and environmental conditions, geometrical tolerances, numerical and/or modelling errors. Therefore, uncertainty quantification (UQ) methods are required, in order to assess the effects of uncertain parameters on the relevant outputs. Earlier uncertainty studies addressed deterministic uncertainty analysis (UA) for numerical and modelling errors [1, 2, 3]. More recently, the research moved to stochastic UQ for environmental and operating conditions. Stochastic UQ studies using high-fidelity simulations for ship hydrodynamic problems have been presented in [4, 5, 6, 7].

In design optimization, high-fidelity solvers and UQ methods are integrated with single/multi-objective local/global minimization/maximization algorithms, which may require a large number of computer simulations (and high computational cost) in order to converge to the final solution [7, 8, 9]. UQ and design optimization with high-fidelity solvers still represent a technological challenge and require efficient methods and implementations.

In order to reduce the computational cost, metamodelling methods have been developed and successfully applied in several engineering fields [10, 11, 12]. In addition to metamodels, multi-fidelity approximation methods have been developed with the aim of combining to some extent the accuracy of high-fidelity solvers with the computational cost of low-fidelity solvers [13, 14, 15], or the accuracy of experiments (high-fidelity data) and computer simulations (low-fidelity) [16]. Multi-fidelity approximations for uncertainty quantification have been successfully investigated in [17] and applied in maritime [18] and industrial problems [19]. Furthermore, multi-fidelity metamodels have been successfully used for design optimization [20, 21, 22].

The objective of the present work is to present a multi-fidelity global metamodel, which manages high- and low-fidelity solvers through a multi-fidelity adaptive sampling procedure. The method is developed as an essential part of efficient uncertainty quantification of computationally expensive computer simulations. The current method is an extension to multiple functions [23] of the work presented in [24].

The multi-fidelity approximation is built as the sum of a low-fidelity-trained metamodel and the metamodel of the difference (error) between high- and low-fidelity evaluations. The metamodel is based on the dynamic stochastic radial basis function (RBF) method, presented in [23] for uncertainty quantification and extended to design optimization in [25]. The method provides the prediction and the associated uncertainty. The adaptive sampling procedure is driven by the maximum absolute value of the uncertainty, evaluated for each multi-fidelity metamodel. The prediction uncertainty of both the low-fidelity and the error metamodel is used for the adaptive refinement of the low- and high-fidelity training sets. High- or low-fidelity simulations are computed, depending on the relative uncertainty of error and low-fidelity metamodels.

The method is applied to a steady fluid-structure interaction (FSI) problem, used as a benchmark both for experimental [26] and simulation-based shape design optimization studies, using high-fidelity solvers [27]. Herein, the performances of the 3D NACA 0009 stainless steel hydrofoil are addressed in terms of lift and drag coefficients versus the angle of attack (AoA) and the Reynolds number (Re). Two problems are presented. The first problem addresses lift and drag coefficients using high- and low-fidelity simulations. Specifically, high-fidelity evaluations are provided by steady FSI simulations and low-fidelity evaluations are given by

steady hydrodynamic simulations with fixed geometry. The second problem addresses the same functions using available experimental data [26] as high-fidelity evaluations. Both high- and low-fidelity simulations are performed by finite element method (FEM) using the commercial code COMSOL Multiphysics^{TM}. A preliminary structural and hydrodynamic characterization of the current hydrofoil has been provided in [28].

2 MULTI-FIDELITY ADAPTIVE METAMODEL

Considering n functions (relevant outputs), the multi-fidelity metamodel is defined as

$$\begin{aligned} \hat{f}_i(\mathbf{x}) &= \tilde{f}_{i,L}(\mathbf{x}) + \tilde{\delta}_i(\mathbf{x}),\ i = 1, \ldots, n \\ \delta_i(\mathbf{x}) &= f_{i,H}(\mathbf{x}) - f_{i,L}(\mathbf{x}),\ i = 1, \ldots, n \end{aligned} \tag{1}$$

where $\mathbf{x} \in \mathbb{R}^n$ is the independent variable (uncertain parameter), superscript $\sim$ denotes the RBF prediction, and δ_i is the difference (error) between high- and low-fidelity simulations (respectively, $f_{i,H}$ and $f_{i,L}$ with $i = 1, \ldots, n$).

The uncertainty associated with the prediction provided by the multi-fidelity metamodel of the i-th function is defined as

$$U_{\hat{f}_i}(\mathbf{x}) = \sqrt{U^2_{\tilde{f}_{i,L}}(\mathbf{x}) + U^2_{\tilde{\delta}_i}(\mathbf{x})} \tag{2}$$

where $U_{\tilde{f}_{i,L}}$ and $U_{\tilde{\delta}_i}$ are the uncertainties associated to the prediction of the i-th function, provided by the low-fidelity and error metamodels ($\tilde{f}_{i,L}$ and $\tilde{\delta}_i$), respectively [23].

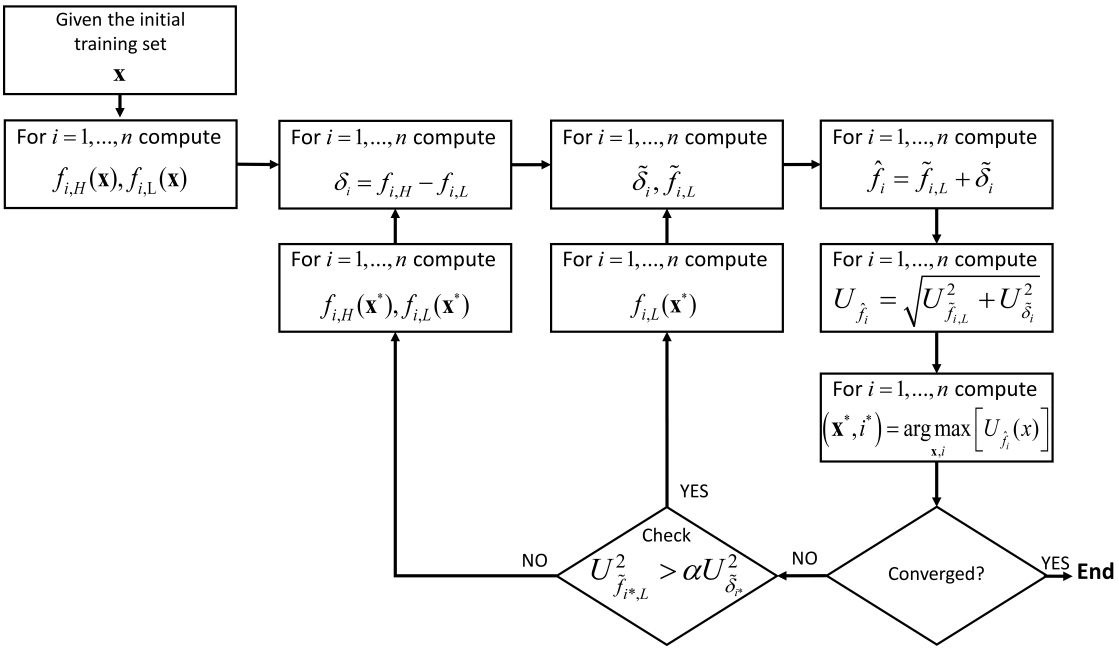

Figure 1: Multi-fidelity metamodel adaptive sampling procedure.

The multi-fidelity metamodel is trained using the adaptive procedure shown in Fig. 1. After initialization, a new sample is added to the training set at each iteration, solving the following

problem:

$$(\mathbf{x}^*, i^*) = \underset{\mathbf{x},i}{\operatorname{argmax}}[U_{\hat{f}_i}(\mathbf{x})] \tag{3}$$

Once $\mathbf{x}^*$ and i^* are evaluated, the training sets H and/or L (high- and low-fidelity, respectively) are updated as

$$\begin{cases} \text{If } U^2_{\tilde{f}_{i^*,L}}(\mathbf{x}^*) \geq \alpha U^2_{\tilde{\delta}_{i^*}}(\mathbf{x}^*), \text{ then add } \mathbf{x}^* \text{ to } L \\ \text{If } U^2_{\tilde{f}_{i^*,L}}(\mathbf{x}^*) < \alpha U^2_{\tilde{\delta}_{i^*}}(\mathbf{x}^*), \text{ then add } \mathbf{x}^* \text{ to } H \text{ and } L \end{cases} \tag{4}$$

where $\alpha \in$[0, 1] is an arbitrary tuning parameter, related to the ratio of the computational cost of the low- and high-fidelity simulations.

3 STOCHASTIC RADIAL BASIS FUNCTIONS

The prediction $\tilde{f}$ is evaluated as the expected value of a set of stochastic RBF predictions [23], which depend on the stochastic parameter $\epsilon \sim \text{unif}[1, 3]$:

$$\tilde{f}(\mathbf{x}) = E[g(\mathbf{x}, \epsilon)]_\epsilon \tag{5}$$

with

$$g(\mathbf{x}, \epsilon) = \sum_{i=1}^{m} w_i \, \varphi(\mathbf{x} - \mathbf{x}_i) \tag{6}$$

where m is the size of the training set, $\mathbf{x}_i$ are the training points, $\varphi(\cdot) = \|\cdot\|^\epsilon$, and $\|\cdot\|$ is the Euclidean norm. The coefficients w_i are obtained by the linear system $\mathbf{A}\mathbf{w} = \mathbf{y}$ with $\mathbf{w} = \{w_i\}$. The elements of the matrix $\mathbf{A}$ are $a_{ij} = \varphi(\mathbf{x}_i - \mathbf{x}_j)$ and the vector $\mathbf{y} = \{y_i\}$ collects the function evaluations at the training points, $y_i = f(\mathbf{x}_i)$.

The uncertainty associated to the metamodel prediction, $U(\mathbf{x})$, is quantified at each $\mathbf{x}$ as the 95%-confidence interval of $g(\mathbf{x}, \epsilon)$. This may be evaluated using a Monte Carlo sampling over ϵ, as shown in [23].

4 APPLICATION: NACA 0009 STAINLESS STEEL HYDROFOIL

The FSI problem presented by [26] is used herein to demonstrate the method. Specifically, the performances of a 3D NACA 0009 stainless steel hydrofoil are addressed in terms of lift and drag coefficients (C_L, C_D). C_L, C_D are evaluated versus AoA and Re (2D problem), respectively varying within [-1, 15] deg and [2E5, 6E5], which represent a subdomain of experimental data provided by [26] (AoA $\in$ [-15, 15] deg and Re $\in$ [2E5, 1E6]). Both the range of variation have been selected according to the outcomes provided by [26]. Specifically, it was observed that pre-stall forces are Re dependent only for Re$\leq$8E5 (although the dependence is weak).

The model main particulars are: root, mid and tip chords respectively equal to 0.12 m, 0.09 m and 0.06 m, and span length equal to 0.3 m. The resulting aspect ratio is 3.33. According to [26], a stainless steel with a density of 7900 kg/m^3, a Young modulus of 193 GPa and a Poisson modulus of 0.3 is chosen for the hydrofoil. Water density and dynamic viscosity are set equal to 999 kg/m^3 and 1.1545E–3 Pa·s, whereas the absolute pressure and temperature are set to 201.13 kPa and 293.15 K.

Figures 2(a) and 2(b) respectively show the experimental values of lift and drag coefficients, provided by [26], versus AoA for Re=$\{$2E5;4E5;6E5$\}$. The peak of the lift coefficient falls within 10 and 11 deg, showing stall for AoA$>$11 deg.

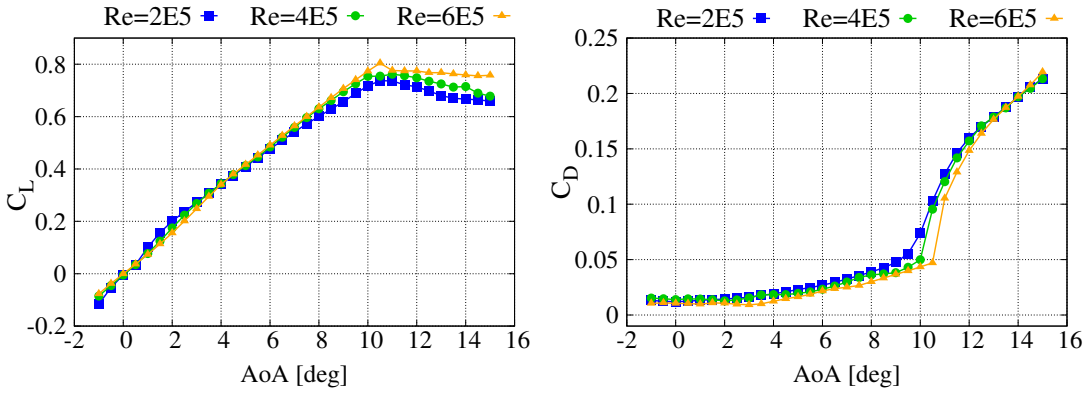

(a) Lift coefficient versus AoA

(b) Drag coefficient versus AoA

Figure 2: Experimental lift and drag coefficients for several Reynolds numbers [26].

Two problems are solved. In the first problem (namely problem 1) high-fidelity evaluations are provided by FSI simulations, performed with a two-way stationary coupling between hydrodynamic (steady incompressible Reynolds Averaged Navier-Stokes Equations, RANSE) and structural simulations. The low-fidelity evaluations are obtained through steady incompressible RANSE hydrodynamic simulations, with rigid hydrofoil. Both high- and low-fidelity simulations are performed using the commercial FEM-based code COMSOL Multiphysics^{TM} and the ratio between the computational time of the low- and the high-fidelity simulations is approximately equal to 0.2, see Tab. 1.

In the second problem (namely problem 2), the high-fidelity evaluations are provided by available experimental data from [26]. Therefore, the multi-fidelity metamodel is initially trained with experimental data and low-fidelity simulations. For this problem, the ratio between the computational time of the high-fidelity evaluations and the low-fidelity simulations is set to infinite, implying that only low-fidelity evaluations are used to update the multi-fidelity metamodel.

5 SIMULATION SETUP

FSI and hydrodynamic simulations share the same *C*-type domain for the hydrodynamics. A length equal to four mid-chords (C_m) is used as radius of the *C*, the total height of the domain is twice the span of the hydrofoil. Downstream, the domain extends ten times the mid-chord, see Fig. 3(a).

The domain is discretized with a structured mesh and the distribution of the elements in the downstream region is intentionally refined to guarantee the finest discretization of wake flow for each AoA of the hydrofoil. The grid is also refined in critical regions such as the root and the tip of the hydrofoil, Fig. 3(b). Parameters pertaining to the grid size used for high- and low-fidelity simulations are summarized in Tab. 1. Note that high-fidelity (FSI) simulations also include the structural grid (with coincident nodes) and associated degrees of freedom.

The $k-\epsilon$ turbulence model is used with standard coefficients [29] and wall function. The non-linear stationary problem is solved with a dumped Newton method through linear step [30]. A pseudo time-stepping is introduced to increase the simulation stability. The Courant-Friedrichs-Lewy (CFL) number adjusts the local time-step according to $\Delta t_{loc} = CFL_{loc}h/U$, where h is the longest cell edge, and U is the magnitude of the local fluid flow velocity. The

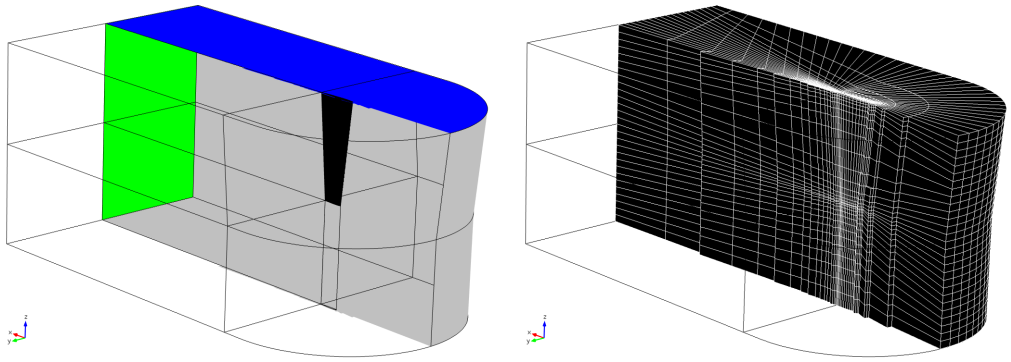

(a) Hydrodynamic domain and boundary conditions

(b) Meshed *C*-type domain

Figure 3: Hydrodynamic domain and grid.

Simulation	N. of elements	DoFs	Simulation time [h]
FSI	31.3k	2M	≈ 10
Hydrodynamic	29.7k	1.2M	≈ 2

Table 1: Summary of the simulation parameters.

CFL is decreased, proportionally with the increase of the AoA, starting from the value CFL=1.

Second order shape functions are used for the displacement vector, mesh deformation (if any), velocity, turbulent kinetic energy and turbulent dissipation rate. First order shape functions are used for the pressure.

The hydrodynamic boundary conditions are set considering an inlet/undisturbed flow on the gray face, a wall on the blue face and an outlet on the green face. The black faces represent the hydrofoil (elastic/rigid wall), see Fig. 3(a).

5.1 High-Fidelity Simulations: Fluid-Structure Interaction Solver

The structural boundary conditions include null displacement and rotation at the root section of the hydrofoil. The hydroelastic deformation of the hydrofoil implies the deformation of the mesh. In COMSOL Multiphysics^{TM} arbitrary Lagrangian-Euler (ALE) method is implemented. The Yeoh method is applied, with a stiffness factor equal to 150 [31].

A segregated iterative solver is applied in order to reduce the problem dimension. Specifically, three segregated groups are defined: the first for the displacement vector, the second for the spatial coordinates of the deformed mesh, and the third for the velocity, pressure, turbulent kinetic energy and turbulent dissipation rate.

The displacement vector is solved with a direct MUltifrontal Massively Parallel Solver (MUMPS) [31]. The others segregated groups are solved using the Flexible Generalized Minimal Residual Method (FGMRES) [32], preconditioned with Generalized Minimal Residual Method (GMRES) [33].

5.2 Low-Fidelity Simulations: Hydrodynamic Solver Only

Two segregated groups are solved: the first for velocity and pressure, and the second for turbulent kinetic energy and turbulent dissipation rate. Both segregated groups are solved using

the FGMRES, preconditioned with GMRES.

6 NUMERICAL RESULTS

The pressure contour on the hydrofoil and on the half-span plane are shown for both FSI and hydrodynamic-only simulations, for AoA=7 deg, Re=4E5, respectively in Figs. 4(a) and 4(b). In particular, the deflection of the tip of the hydrofoil is evident in Fig. 4(a).

Figure 5(a) shows for the FSI simulation the pressure contour on the hydrofoil and on the half-span plane, along with the streamlines deformed by the local velocity component (left color legend). Finally, Fig. 5(b) shows the pressure contour on the hydrofoil and the velocity contour on the half-span plane, along with the streamlines deformed by the local velocity component (left color legend).

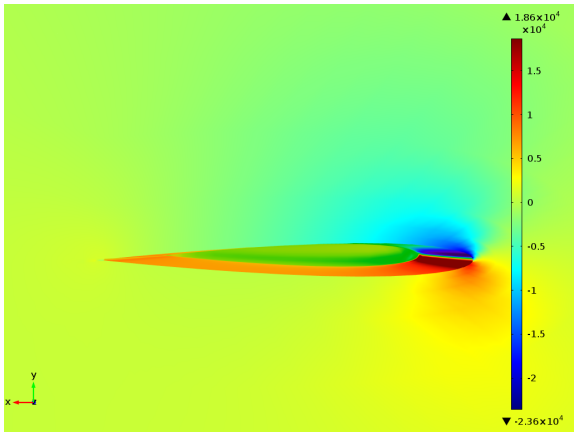

(a) FSI simulation. Pressure contour on hydrofoil and half-span plane

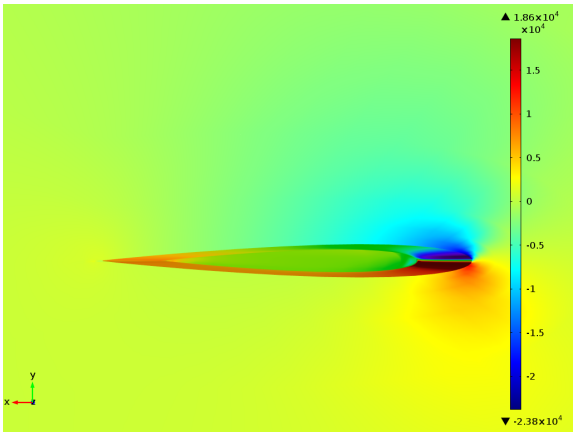

(b) Hydrodynamic-only simulation. Pressure contour on hydrofoil and half-span plane

Figure 4: High- and low-fidelity simulations, AoA=7 deg, Re=4E5.

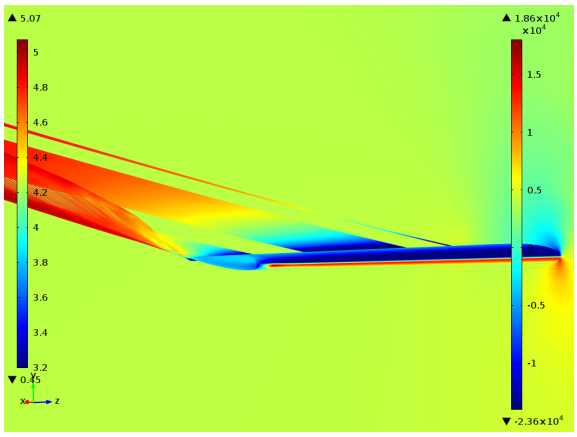

(a) FSI simulation. Pressure contour on hydrofoil and half-span plane

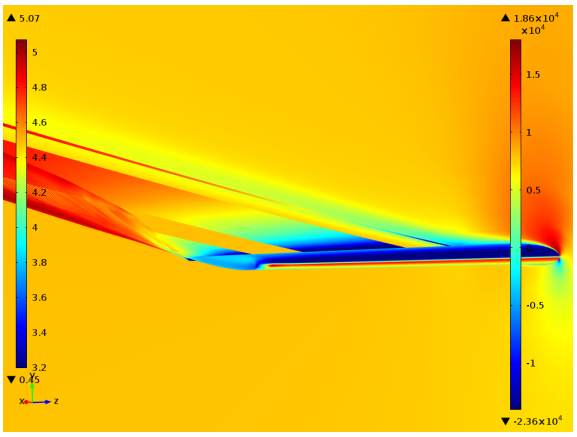

(b) FSI simulation. Pressure contour on hydrofoil and velocity contour on half-span plane

Figure 5: High-fidelity simulation, AoA=7 deg, Re=4E5.

The numerical results that follow are presented showing the maximum value of the uncertainty of the multi-fidelity metamodel, normalized with respect to the function range (R). The

adaptive sampling procedure is assumed at convergence when the maximum value of the uncertainty does not change significantly, if new simulations are added. Furthermore, the multi-fidelity metamodel, along with the uncertainty of the low-fidelity and error metamodels are shown at the initial and final iterations. Non-dimensional variables are used to build the metamodel. However, for the sake of clarity, dimensional results are shown. The initial training set is composed by the extreme values of the domain and the central point: AoA={-1;7;15} deg, permuted with Re={2E5;4E5;6E5}.

6.1 Problem 1

Figure 6 shows the maximum value of the normalized uncertainty of the multi-fidelity metamodel versus the computational cost. The maximum value of the uncertainty of the multi-fidelity metamodel of the lift coefficient shows a significant reduction during the iterative process, as shown in Fig. 6(a). The maximum value of the uncertainty of the multi-fidelity metamodel of the drag coefficient shows a quite sudden reduction after 4 iterations, as shown in Fig. 6(b). The convergence of the multi-fidelity metamodel is achieved after 13 iterations, corresponding to about 140 hours of simulation time (wall clock, using 1 Intel Xeon E5-1620 v2 3.9 GHz with 4 cores in parallel). A total of 9 high-fidelity and 20 low-fidelity simulations are used, as summarized in Tab. 2.

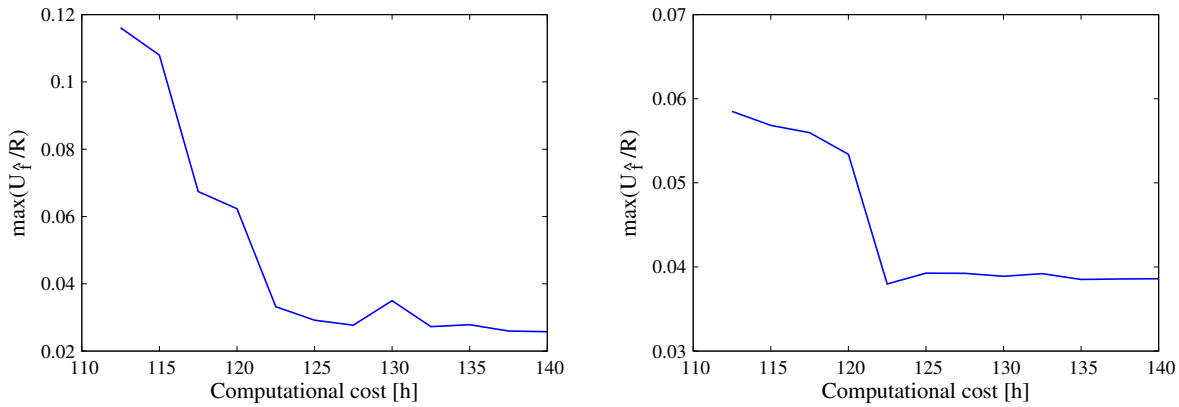

(a) Lift coefficient (b) Drag coefficient

Figure 6: Problem 1, maximum multi-fidelity metamodel uncertainty versus computational cost.

Figures 7(a)-(b), (c)-(d), and (e)-(f) show the initial multi-fidelity metamodel, the low-fidelity and error metamodel uncertainties, respectively for the lift and drag coefficients. The squares and triangles represent the points where the high- (H) and low-fidelity (L) simulations are computed.

Comparing Figs. 7(c) and 7(d) it is worth noting that the uncertainty associated to the low-fidelity metamodel of the lift coefficient is one order of magnitude greater than the uncertainty associated to the low-fidelity metamodel of the drag coefficient.

Figures 8(a)-(b), (c)-(d), and (e)-(f) show the multi-fidelity metamodel, the low-fidelity and error metamodel uncertainties, respectively for the lift and drag coefficients, corresponding to the final iteration (13-th iteration).

It should be noted that the uncertainty of the low-fidelity metamodel is significantly lower than in Figs. 7(c) and 7(d). Figures 8(e) and 8(f) show the uncertainty of the error metamodel, which is not changed, since high-fidelity simulations are not added to the original training set.

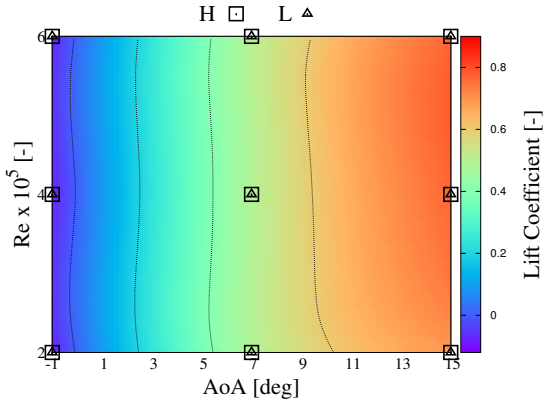

(a) Multi-fidelity metamodel of the lift coefficient

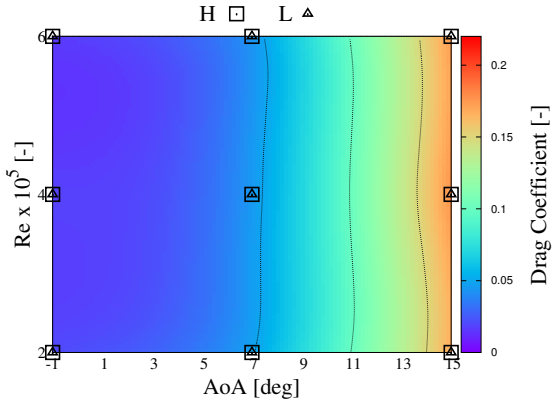

(b) Multi-fidelity metamodel of the drag coefficient

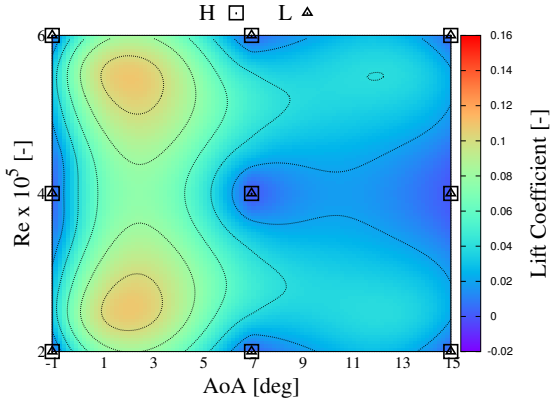

(c) Uncertainty of the low-fidelity metamodel of the lift coefficient

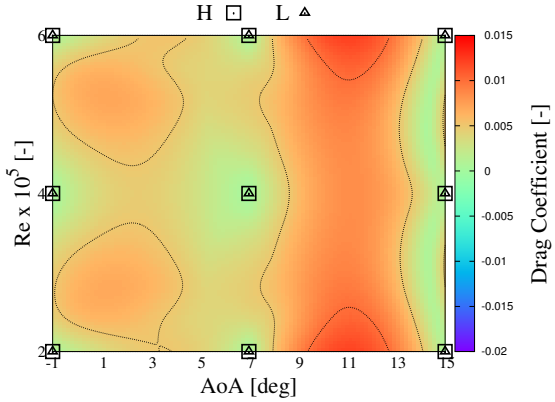

(d) Uncertainty of the low-fidelity metamodel of the drag coefficient

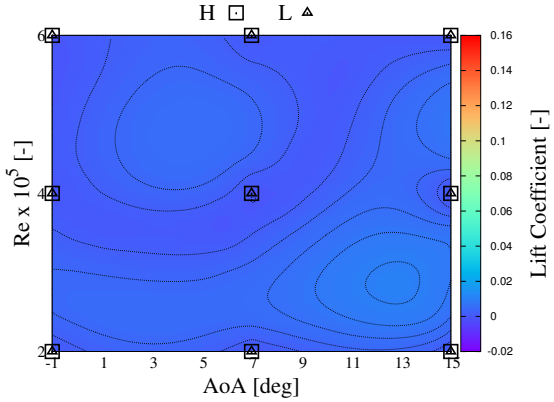

(e) Uncertainty of the error metamodel of the lift coefficient

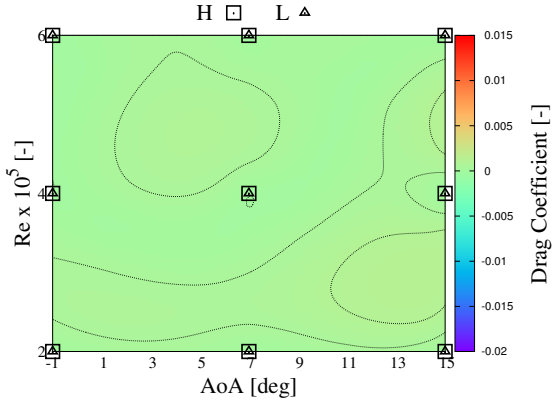

(f) Uncertainty of the error metamodel of the drag coefficient

Figure 7: Problem 1, initial iteration.

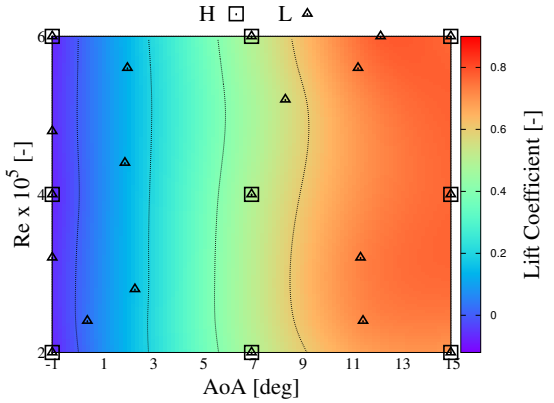

(a) Multi-fidelity metamodel of the lift coefficient

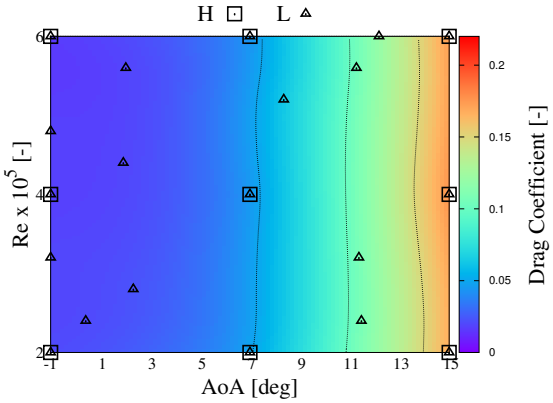

(b) Multi-fidelity metamodel of the drag coefficient

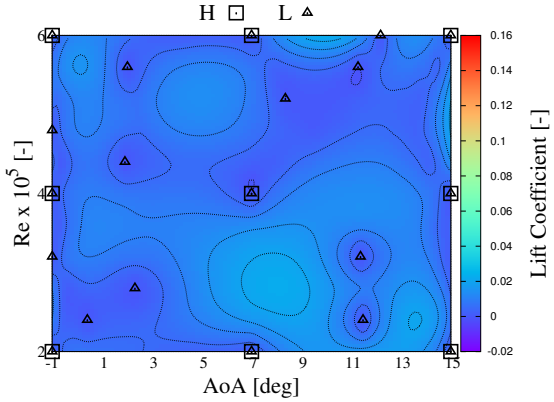

(c) Uncertainty of the low-fidelity metamodel of the lift coefficient

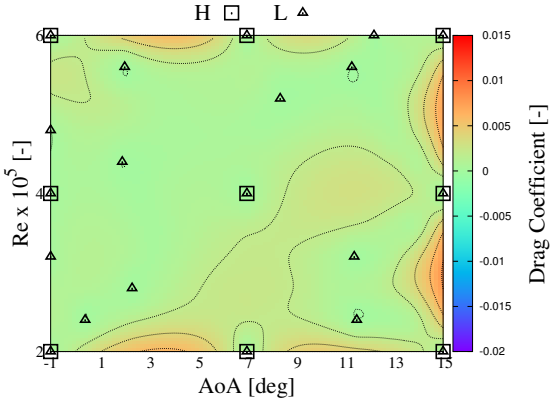

(d) Uncertainty of the low-fidelity metamodel of the drag coefficient

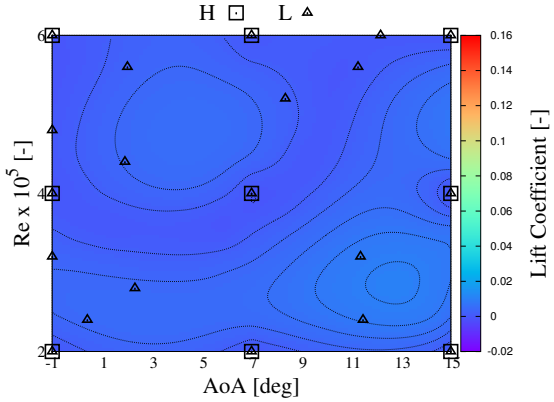

(e) Uncertainty of the error metamodel of the lift coefficient

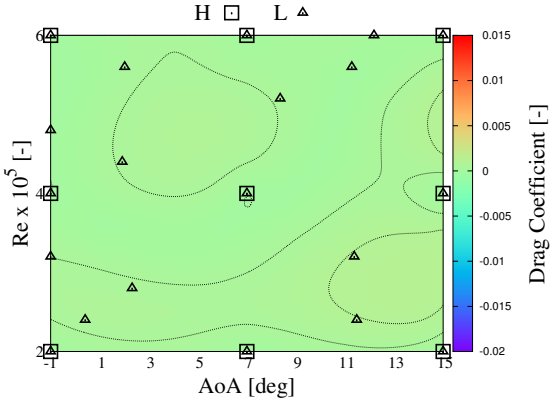

(f) Uncertainty of the error metamodel of the drag coefficient

Figure 8: Problem 1, final iteration.

6.2 Problem 2

Figure 9 shows the maximum value of the uncertainty of the multi-fidelity metamodel versus the computational cost. Figure 9(a) shows the reduction of the maximum value of the uncertainty of the multi-fidelity metamodel of the lift coefficient. The maximum value of the uncertainty of the multi-fidelity metamodel of the drag coefficient shows a quite sudden reduction after 3 iterations, see Fig. 9(b). The convergence of the multi-fidelity metamodel is achieved after 7 iterations, corresponding to about 130 hours of simulation time (wall clock, using 1 Intel Xeon E5-1620 v2 3.9 GHz with 4 cores in parallel). A total of 9 high-fidelity experimental data and 16 low-fidelity simulations are used, as summarized in Tab. 2.

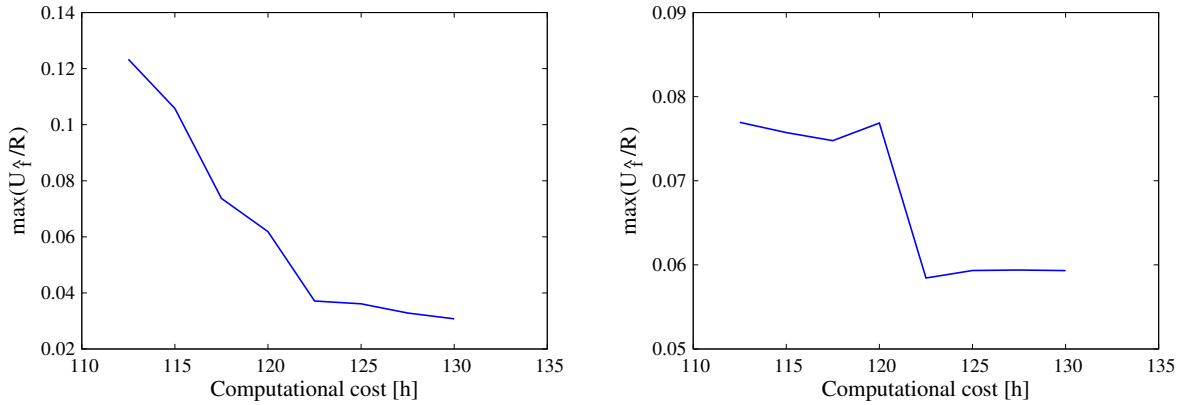

(a) Lift coefficient (b) Drag coefficient

Figure 9: Problem 2, maximum multi-fidelity metamodel uncertainty versus computational cost.

Figures 10(a)-(b), (c)-(d), and (e)-(f) show the initial multi-fidelity metamodel, the low-fidelity and error metamodel uncertainties, respectively for lift and drag coefficients. The squares represent high-fidelity experimental data (H) and the triangles represent the points where low-fidelity (L) simulations are computed.

Considering Figs. 10(c) and 10(d) it should be noted that the uncertainty associated to the low-fidelity metamodel of the lift coefficient is one order of magnitude greater than the uncertainty associated to the low-fidelity metamodel of the drag coefficient. Figures 10(e) and 10(f) show the uncertainty of the error metamodel, which is considerably greater than the corresponding uncertainties of Figs. 7(e) and 7(f). This effect is due to the difference between the simulations and the experiments, which is significantly greater than the difference between the high- and low-fidelity simulations.

Figures 11(a)-(b), (c)-(d), and (e)-(f) show the multi-fidelity metamodel, the low-fidelity and error metamodel uncertainties, respectively for lift and drag coefficients, at the final iteration (8-th iteration).

It is worth noting that the uncertainty of the low-fidelity metamodel, Figs. 11(c) and 11(d), is significantly lower than in Figs. 10(c) and 10(d), and that the uncertainty of the error metamodel is not changed, since no experimental data is added to the training set.

7 CONCLUSIONS

A multi-fidelity global metamodel has been presented for uncertainty quantification of computationally expensive computer simulations. High- and low-fidelity solvers are used for the metamodel training and managed through an adaptive sampling procedure. Multiple functions

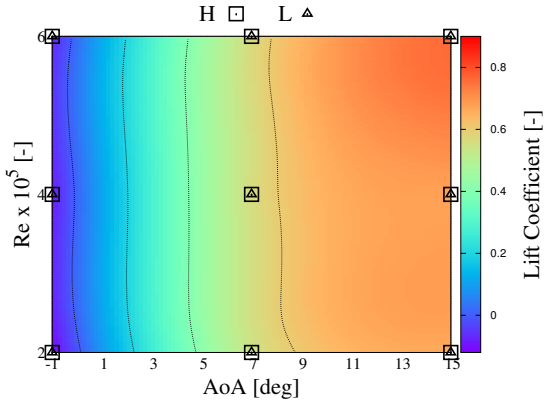

(a) Multi-fidelity metamodel of the lift coefficient

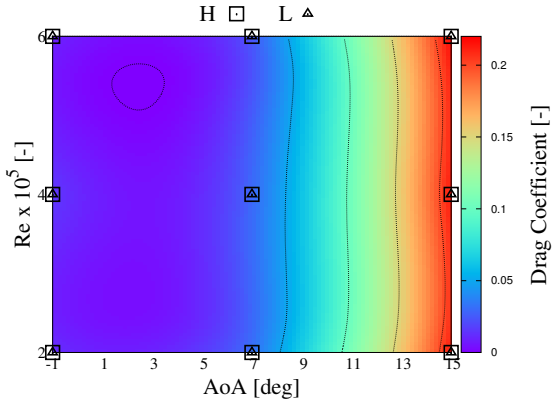

(b) Multi-fidelity metamodel of the drag coefficient

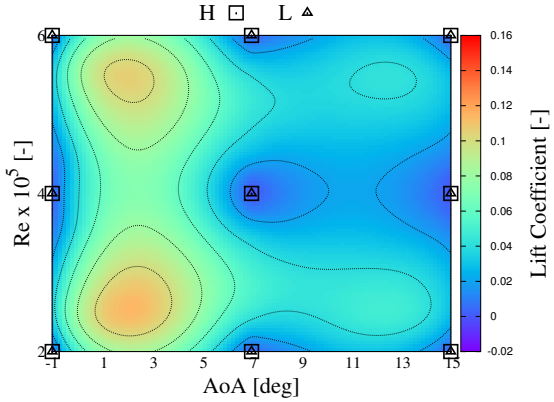

(c) Uncertainty of the low-fidelity metamodel of the lift coefficient

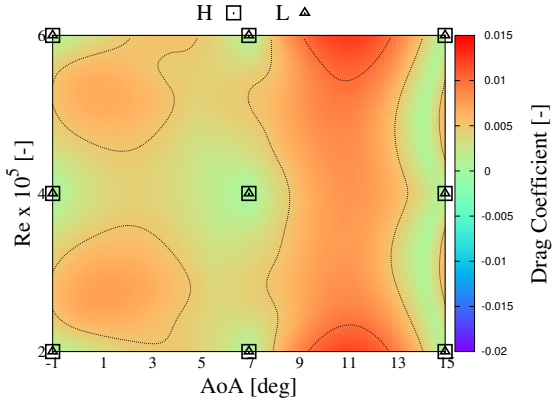

(d) Uncertainty of the low-fidelity metamodel of the drag coefficient

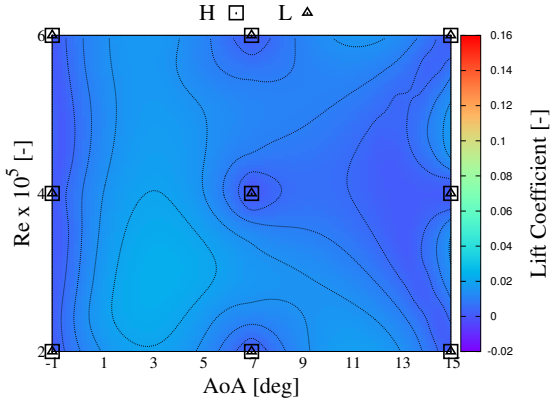

(e) Uncertainty of the error metamodel of the lift coefficient

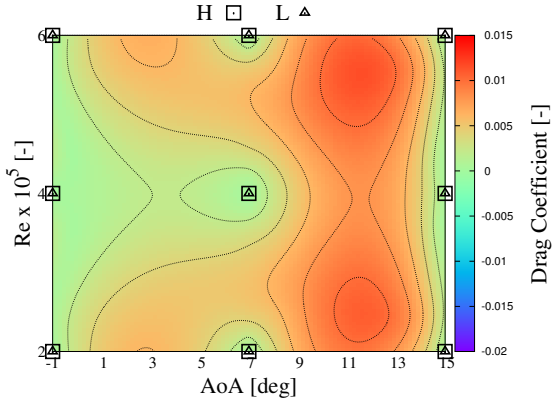

(f) Uncertainty of the error metamodel of the drag coefficient

Figure 10: Problem 2, initial iteration.

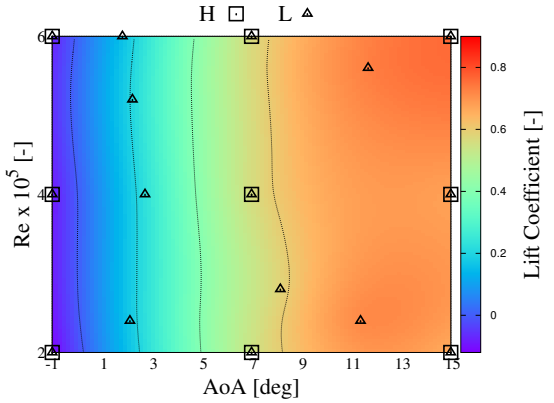

(a) Multi-fidelity metamodel of the lift coefficient

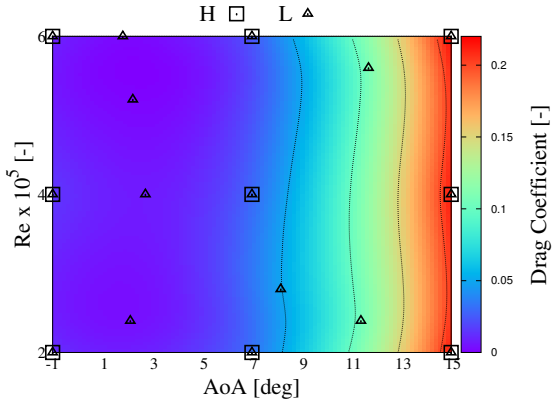

(b) Multi-fidelity metamodel of the drag coefficient

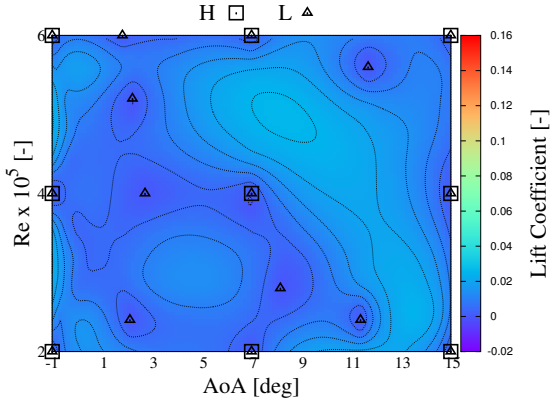

(c) Uncertainty of the low-fidelity metamodel of the lift coefficient

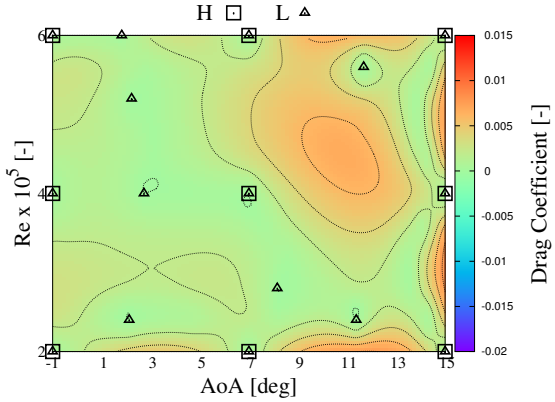

(d) Uncertainty of the low-fidelity metamodel of the drag coefficient

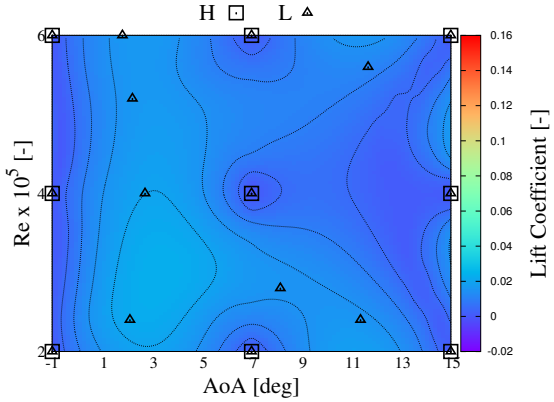

(e) Uncertainty of the error metamodel of the lift coefficient

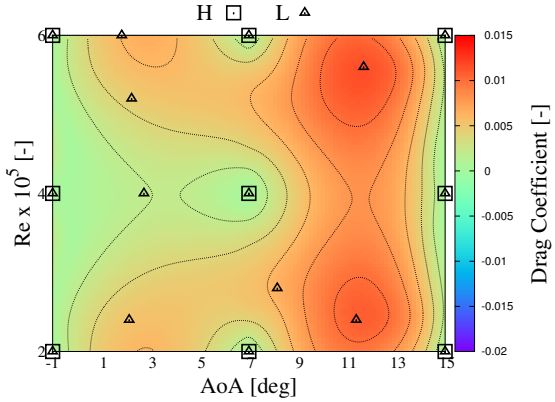

(f) Uncertainty of the error metamodel of the drag coefficient

Figure 11: Problem 2, final iteration.

Pr.			Initial iteration				Final iteration	
			C_L	C_D			C_L	C_D
#	H	L	$\max(U_{\hat{f}}/R)$	$\max(U_{\hat{f}}/R)$	H	L	$\max(U_{\hat{f}}/R)$	$\max(U_{\hat{f}}/R)$
1	9	9	0.1161	0.0585	9	20	0.0254	0.0386
2	9	9	0.1233	0.0769	9	16	0.0307	0.0593

Table 2: High (H) and low (L) fidelity evaluations and $\max(U_{\hat{f}}/R)$ at the initial and final iterations.

have been considered, simultaneously. The multi-fidelity approximation is obtained as the sum of a low-fidelity-trained metamodel and the metamodel of the difference (error) between high- and low-fidelity evaluations. The metamodel is based on the dynamic stochastic RBF method, which provides the prediction and the associated uncertainty. The prediction uncertainty of both the low-fidelity and the error metamodel is used for the adaptive refinement of the low- and high-fidelity training sets, respectively.

The method has been applied to a steady FSI problem addressing the lift and drag coefficients of a 3D NACA 0009 stainless steel hydrofoil. Two problems have been presented: the first with high-fidelity evaluations provided by steady FSI simulations and the second with high-fidelity evaluations provided by experimental data. Low-fidelity evaluations have been provided by hydrodynamic simulations for both problems.

For problem 1, the overall uncertainty of the multi-fidelity metamodels has been reduced achieving 2.5% and 3.8% (of the function range) for the lift and drag coefficient, respectively. For problem 2, an uncertainty of 3% and 5.9% for the lift and drag coefficient has been achieved, respectively. Although the overall uncertainty in Problem 1 is lower than in problem 2, a better agreement with the experimental results is obtained using experimental data in the initial training set as in problem 2. Furthermore, less iterations have been used for problem 2. For both problems 1 and 2, the adaptive sampling method always required low-fidelity evaluations and no high-fidelity information was added to the model after the initialization. This is due to the high cost of high-fidelity evaluations (simulations or experiments) and the small uncertainty associated to the error between low- and high-fidelity functions.

Future work will extend the current study to different (and more flexible) materials, such as aluminum and/or composite materials, and will also include the application of the method to separate and combined problems of uncertainty quantification and design optimization.

Acknowledgments

The present research is supported by the Italian Flagship Project RITMARE, coordinated by the Italian National Research Council and funded by the Italian Ministry of Education, University and Research, within the National Research Program 2011-2013. The authors are also grateful to Dr Woei-Min Lin and Dr Ki-Han Kim of the US Navy Office of Naval Research, for their support through NICOP grant N62909-15-1-2016.

REFERENCES

[1] F. Stern, R.V. Wilson, H.W. Coleman, E.G. Paterson, "Comprehensive approach to verification and validation of CFD simulations–Part 1: Methodology and Procedures," *ASME J. Fluids Eng.*, **123**(4), 793–802, 2001.

[2] F. Stern, R.V. Wilson, J. Shao, "Quantitative approach to V&V of CFD simulations and certification of CFD codes," *Int. J. Numer. Meth. Fluids*, **50**, 1335–1355, 2006.

[3] T. Xing, F. Stern, "Factors of safety for Richardson extrapolation," *ASME J. Fluids Eng.*, **132**(6), 2010.

[4] S.M. Mousaviraad, W. He, M. Diez, F. Stern, "Framework for convergence and validation of stochastic uncertainty quantification and relationship to deterministic verification and validation," *International Journal for Uncertainty Quantification*, **3**(5), 2013.

[5] M. Diez, W. He, E.F. Campana, F. Stern, "Uncertainty quantification of Delft catamaran resistance, sinkage and trim for variable Froude number and geometry using metamodels, quadrature and Karhunen-Loève expansion", *Journal of Marine Science and Technology*, **19**(2), 143–169, 2014.

[6] W. He, M. Diez, Z. Zou, E.F. Campana, F. Stern, "URANS study of Delft catamaran total/added resistance, motions and slamming loads in head sea including irregular wave and uncertainty quantification for variable regular wave and geometry", *Ocean Engineering*, **74**, 189–217, 2013.

[7] M. Diez, X. Chen, E.F. Campana, F. Stern, "Reliability-based robust design optimization for ships in real ocean environment", *Proc. 12th International Conference on Fast Sea Transportation, FAST*, Amsterdam, The Netherlands, December 2-5, 2013.

[8] M. Diez, E.F. Campana, F. Stern, "Development and evaluation of hull-form stochastic optimization methods for resistance and operability", *Proc. 13th International Conference on Fast Sea Transportation, FAST*, Washington D.C., USA, September 1-4, 2015.

[9] Y. Tahara, M. Diez, S. Volpi, X. Chen, E.F. Campana, F. Stern, "CFD-based multiobjective stochastic optimization of a waterjet propelled high speed ship", *Proc. 30th Symposium on Naval Hydrodynamics*, Hobart Tasmania, Australia, November 2-7, 2014.

[10] T. W. Simpson, J. Poplinski, P. N. Koch, J. K. Allen, "Metamodels for computer-based engineering design: survey and recommendations," *Engineering with computers*, **17**(2), 129–150, 2001.

[11] R. Jin, W. Chen, T. W. Simpson, "Comparative studies of metamodelling techniques under multiple modelling criteria," *Structural and Multidisciplinary Optimization*, **23**(1), 1–13, 2001.

[12] N. V. Queipo, R. T. Haftka, W. Shyy, T. Goel, R. Vaidyanathan,P. Kevin Tucker, "Surrogate-based analysis and optimization," *Progress in aerospace sciences*, **41**(1), 1–28, 2005.

[13] N. Alexandrov, E. Nielsen, R. Lewis, W. Anderson, "First-order model management with variable-fidelity physics applied to multi-element airfoil optimization," *AIAA paper*, 4886, 2000.

[14] N. M. Alexandrov, R. M. Lewis, C. R. Gumbert, L. L. Green, P. A. Newman, "Approximation and model management in aerodynamic optimization with variable-fidelity models," *Journal of Aircraft*, **38**(6), 1093–1101, 2001.

[15] T. W. Simpson, V. Toropov, V. Balabanov, F. A. Viana, "Design and analysis of computer experiments in multidisciplinary design optimization: a review of how far we have come or not," in *12th AIAA/ISSMO Multidisciplinary Analysis and Optimization Conference*, **5**(10), 10–12, 2008.

[16] Y. Kuya, K. Takeda, X. Zhang, A. I. J. Forrester, "Multifidelity Surrogate Model of Experimental and Computational Aerodynamic Data Sets," *AIAA Journal*, **49**(2), 289–298, 2011.

[17] L. W. T. Ng, M. Eldred, "Multifidelity uncertainty quantification using nonintrusive polynomial chaos and stochastic collocation," in *Proceedings of the 14th AIAA Non-Deterministic Approaches Conference, number AIAA-2012-1852*, Honolulu, HI, **43**, 2012.

[18] J. de Baar, S. Roberts, R. Dwight, B. Mallol, "Uncertainty quantification for a sailing yacht hull, using multi-fidelity kriging," *Computers & Fluids*, **123**, 185–201, 2015.

[19] A. S. Padrón, J. J. Alonso, F. Palacios, M. Barone, M. S. Eldred, "Multi-fidelity uncertainty quantification: application to a vertical axis wind turbine under an extreme gust," in *15th AIAA/ISSMO Multidisciplinary Analysis and Optimization Conference*, Atlanta, GA, USA, 2014.

[20] A. Nelson, J. J. Alonso, T. H. Pulliam, "Multi-fidelity aerodynamic optimization using treed meta-models," in *25th AIAA Applied Aerodynamics Conference*, Miami, 25–28, 2007.

[21] G. Sun, G. Li, S. Zhou, W. Xu, X. Yang, Q. Li, "Multi-fidelity optimization for sheet metal forming process," *Structural and Multidisciplinary Optimization*, **44**(1), 111–124, 2010.

[22] Q. Zhou, X. Shao, P. Jiang, H. Zhou, L. Shu, "An adaptive global variable fidelity metamodeling strategy using a support vector regression based scaling function," *Simulation Modelling Practice and Theory*, **59**, 18–35, 2015.

[23] S. Volpi, M. Diez, N. J. Gaul, H. Song, U. Iemma, K.K. Choi, E. F. Campana, F. Stern, "Development and validation of a dynamic metamodel based on stochastic radial basis functions and uncertainty quantification," *Structural and Multidisciplinary Optimization*, **51**, 347–368, 2015.

[24] R. Pellegrini, U. Iemma, C. Leotardi, E. F. Campana, M. Diez, "Multi-fidelity Adaptive Global Metamodel of Expensive Computer Simulations", Submitted to *2016 IEEE Congress on Evolutionary Computation*, July, Vancouver, Canada, 2016.

[25] M. Diez, S. Volpi, A. Serani, F. Stern, E. F. Campana, "Simulation-based design optimization by sequential multi-criterion adaptive sampling and dynamic radial basis functions," in *EUROGEN 2015, International Conference on Evolutionary and Deterministic Methods for Design, Optimization and Control with Applications to Industrial and Societal Problems*, Glasgow, UK, September, 2015.

[26] G. A. Zarruk, P. A. Brandner, B. W. Pearce, A. W. Phillips, "Experimental study of the steady fluid-structure interaction of flexible hydrofoils", *Journal of Fluids and Structures*, **51**, 326–343, 2014.

[27] N. Garg, G. K.W. Kenway, Z. Lyu, J. R.R.A. Martins, Y. L. Young "High-fidelity Hydrodynamic Shape Optimization of a 3-D Hydrofoil", *Journal of Ship Research*, **59**(4), 209–226, 2015.

[28] R. Pellegrini, C. Leotardi, U. Iemma, E. F. Campana, M. Diez, "Structural and Hydrodynamic Characterization of a NACA 0009 Hydrofoil by Finite Elements", *18th Numerical Towing Tank Symposium*, Cortona, Italy, September, 2015.

[29] W. Jones, B. Launder, "The prediction of laminarization with a two-equation model of turbulence". *International journal of heat and mass transfer*, **15**(2), 301–314, 1972.

[30] P. Deuflhard, "A modified newton method for the solution of ill-conditioned systems of nonlinear equations with application to multiple shooting", *Numerische Mathematik*, **22**(4), 289–315, 1974.

[31] COMSOL^{TM}, "COMSOL Multiphysics Reference Manual", 2014.

[32] Y. Saad, "A flexible inner-outer preconditioned GMRES algorithm", *SIAM Journal on Scientific Computing*, **14**(2), 461–469, 1993.

[33] Y. Saad, M. H. Schultz, "GMRES: A generalized minimal residual algorithm for solving nonsymmetric linear systems", *SIAM Journal on scientific and statistical computing*, **7**(3), 856–869, 1986.